Supporting Information

Optimal cellular mobility for synchronization arising from the gradual recovery of intercellular interactions

Koichiro Uriu, Saúl Ares, Andrew C. Oates and Luis G. Morelli

Text S1

1. Derivation of the effective coupling strength

Here we derive Eq. (5) in the main text, the time average of the coupling strength between two adjacent sites in a two-dimensional lattice. To illustrate how to calculate the time average of the coupling strength, we consider a time series of the coupling strength between two adjacent sites $\mathbf{k}$ and $\mathbf{k}'$ (*e.g.* $\mathbf{k}=(k, l)$ and $\mathbf{k}'=(k, l+1)$), denoted as $\kappa_{\mathbf{kk}'}(t)$ (figures S2(*A*) and (*B*)). For simplicity, we consider that these two sites are located in the bulk of a two-dimensional lattice.

Figure S2(*B*) shows an example of the time series of $\kappa_{\mathbf{kk}'}(t)$. In figure S2(*B*) the coupling strength $\kappa_{\mathbf{kk}'}(t)$ is reset to zero at times t_0, t_1, t_2, …, t_n, meaning that a cell in either site $\mathbf{k}$ or $\mathbf{k}'$ was replaced by another cell coming from another neighboring site at these time points (*e.g.* the cell in site $(k, l-1)$ exchanges its location with the one in site $\mathbf{k}=(k, l)$). Note that $\kappa_{\mathbf{kk}'}(t)$ is not affected by an exchange of location between the cells in sites $\mathbf{k}$ and $\mathbf{k}'$ (figure 1(*A*) in the main text). We assume that $T=t_n-t_0$ is sufficiently large so that many exchange events occur in this interval making $\kappa_{\mathbf{kk}'}(t)$ go to zero. The waiting times $\tau_i=t_i-t_{i-1}$ (i = 1, 2, …, n) represent the length of the interaction time during which the two cells that met at t_{i-1} in site $\mathbf{k}$ and $\mathbf{k}'$ stay adjacent to each other (figure S2(*B*)). To calculate the time average of $\kappa_{\mathbf{kk}'}(t)$, we first derive the probability density function for the length of the interaction time τ_i. Then, using the probability density function we calculate the time average of $\kappa_{\mathbf{kk}'}(t)$.

S1.1 The probability density function for the length of the interaction time

The probability that the cell in site $\mathbf{k}$ exchanges its location with one of its three neighbors other than the cell in site $\mathbf{k}'$ within the small time interval Δt is $3\lambda\Delta t/4$,

where λ is the moving rate defined in the main text (figure S2(*A*)). The same is valid for the cell in site $\mathbf{k'}$, so the probability that either of these two cells moves away from the other cell in the small time interval Δt can be written as $3\lambda\Delta t/2$. Hence, the probability density function for the length of the interaction time is $f(\tau)=3\lambda e^{-3\lambda\tau/2}/2$. The resulting average interaction time is $\langle\tau\rangle=\int_0^\infty \tau f(\tau)d\tau=1/(3\lambda/2)$.

S1.2 Time average and the effective coupling strength

The time average of $\kappa_{\mathbf{kk'}}(t)$ in time interval $T=t_n-t_0$ is defined as:

$$\langle\kappa\rangle_T=\frac{1}{T}\int_{t_0}^{t_n}\kappa_{\mathbf{kk'}}(t)dt. \tag{S.1.1}$$

The integral in the right hand side of Eq. (S.1.1) can be split in n terms as:

$$\langle\kappa\rangle_T=\frac{1}{T}\left\{\int_{t_0}^{t_1}\kappa(t-t_0)dt+\int_{t_1}^{t_2}\kappa(t-t_1)dt+...+\int_{t_{n-1}}^{t_n}\kappa(t-t_{n-1})dt\right\}, \tag{S.1.2a}$$

where $\kappa(t)=\kappa_0(1-e^{-\beta t})$. Introducing new variables $s_i=t-t_{i-1}$ (i = 1, 2, …, n), Eq. (S.1.2a) reads:

$$\langle\kappa\rangle_T=\frac{1}{T}\sum_{i=1}^{n}\int_0^{\tau_i}\kappa(s_i)ds_i. \tag{S.1.2b}$$

Eq. (S.1.2b) can be re-written as:

$$\langle\kappa\rangle_T=\left(\frac{n}{T}\right)\cdot\left(\frac{1}{n}\sum_{i=1}^{n}\int_0^{\tau_i}\kappa(s_i)ds_i\right). \tag{S.1.3}$$

Because we assumed that T is sufficiently large, the first factor in Eq. (S.1.3) is $n/T=1/\langle\tau\rangle=3\lambda/2$ and the second is:

$$\frac{1}{n}\sum_{i=1}^{n}\int_0^{\tau_i}\kappa(s_i)ds_i\approx\int_0^\infty\left\{\int_0^\tau\kappa(\tau')d\tau'\right\}\frac{3\lambda}{2}e^{-\frac{3\lambda}{2}\tau}d\tau=\int_0^\infty\left\{\int_0^\tau\kappa_0(1-e^{-\beta\tau'})d\tau'\right\}\frac{3\lambda}{2}e^{-\frac{3\lambda}{2}\tau}d\tau.$$

By substituting these equations into Eq. (S. 1.3), we obtain:

$$\langle\kappa\rangle_T\approx\frac{1}{1+3(\lambda/\beta)/2},$$

which is Eq. (5) in the main text. Figure S2(*C*) shows the excellent agreement of Eq. (5) in the main text with the numerically calculated time averages of the coupling strength for $T=300\kappa_0^{-1}$, which gives $n=15\sim15\times10^4$ depending on the value of λ used.

2. Effects of coupling recovery on synchronization in a model with coupling time delays

Previous studies showed that there are time delays in intercellular interactions through Delta-Notch signaling, and that these delays affect the collective dynamics of the segmentation clock [1,2]. For simplicity, in the main text we describe intercellular interactions without including time delays, and focus on the effects of coupling recovery on synchronization. Here we extend the model of the main text to include coupling delays, and study the effects of coupling recovery on synchronization in this extended model.

We introduce the time delay τ_d ($\tau_d > 0$) into Eq. (1a) in the main text as was done in previous studies [1,2]:

$$\frac{d\theta_j(t)}{dt} = \omega_d + \frac{1}{n_j}\sum_{\alpha} \kappa_{j\alpha}(t_{j\alpha}) \sin\left[\theta_\alpha(t-\tau_d) - \theta_j(t)\right] + \sqrt{2C_d}\,\xi_j(t). \quad \text{(S.2.1)}$$

In Eq. (S.2.1) τ_d represents the time required for the phase information of cell α to reach its cell membranes and become visible to cell j. For simplicity, we ignore the time that cell j needs to process the phase information received from cell α. In what follows, the equation for coupling recovery Eq. (1b) in the main text, description of cell movement, and boundary conditions for phase dynamics and cell movement are the same as in the main text. When a cell moves, it carries with it its past history.

To set an initial phase history for each oscillator, its phase value at $t = -\tau_d$ is chosen randomly from a uniform distribution between 0 and 2π. The phase values between $-\tau_d$ and 0 are given by:

$$\theta_j(t) = \omega_d t + \omega_d \tau_d + \theta_j(-\tau_d) \quad \text{for} \quad -\tau_d < t \le 0. \quad \text{(S.2.2)}$$

This initial condition represents a situation where oscillators are not coupled until the time $t = 0$ and at this time point they start to interact with each other. At $t = 0$, the coupling strength for each pair of adjacent cells is set to its maximum capacity κ_0.

We set the values of parameters within the range estimated for the zebrafish segmentation clock [1]: $\kappa_0 = 0.03$ min^{-1}, $\omega_d = 7.33\kappa_0$, and $\tau_d = 0.66\kappa_0^{-1}$, respectively in Eq. (S.2.1). The noise strength C_d is chosen as $C_d = 0.01\kappa_0$. We numerically solved Eq. (S.2.1) with the Euler method together with the Gillespie algorithm for cell movement.

First, we consider the simple case where cells instantaneously establish intercellular interactions after movement (i.e. the coupling recovery rate β in Eq. (1b) in the main text is infinite) to examine the effect of cellular mobility on synchronization

alone under the presence of the coupling time delay (figure S3). When cells do not move (λ = 0, red triangles in figure S3(*B*)), the order parameter $Z(t)$ defined by Eq. (2) in the main text remains very close to zero even after long time. These non-mobile oscillators tend to form local checkerboard patterns where phase values between nearest neighbors are negatively correlated (figures S3(*A*) and (*C*)). These checkerboard patterns are broken at several places due to noise. Accordingly, correlations of phases are rapidly lost with increasing distance (figure S3(*C*)).

In contrast, when cells exchange their locations every $1/4\kappa_0$ on average ($\lambda = 4\kappa_0$, green circles in figure S3(*B*)), the order parameter increases with time and finally reaches a steady state value around one. These mobile oscillators achieve positive and long-range correlation of phases (figure S3(*C*)). Cellular mobility disturbs the formation of local checkerboard patterns and leads to global synchronization across the population of coupled oscillators. When the moving rate is further increased ($\lambda = 40\kappa_0$, blue squares in figure S3(*B*)), global synchronization is realized much faster. Thus, under instantaneous coupling recovery cellular mobility monotonically increases the degree of synchronization in the presence of the coupling time delay, as it does in the model without the delay.

Next, we consider the gradual coupling recovery ($\beta = 33\kappa_0$) after movement together with coupling time delays (figure S4). When $\lambda = 4\kappa_0$, mobility of oscillators still enhances the degree of synchronization compared to the case of non-mobile oscillators (green circles in figures S4(*B*) and (*C*)). Remarkably, when the moving rate becomes higher ($\lambda = 40\kappa_0$), cellular mobility hampers synchronization where neither local nor global phase order exists (figures S4(*A*) and (*C*)). Note that the value of the critical moving rate for synchronization is different from the one for the model without coupling delays, Eq. (8) in the main text. This is because the coupling time delay affects the value of the critical coupling strength together with the noise strength [3]. Nevertheless, these results indicate the existence of the optimal and critical moving rates for synchronization even in the presence of coupling time delays.

References in Supplementary Information

[1] Herrgen L, Ares S, Morelli L G, Schroter C, Julicher F and Oates A C 2010 Intercellular coupling regulates the period of the segmentation clock *Curr Biol* **20** 1244-53

[2] Morelli L G, Ares S, Herrgen L, Schroter C, Julicher F and Oates A C 2009 Delayed coupling theory of vertebrate segmentation *HFSP J* **3** 55-66

[3] Yeung M K S and Strogatz S H 1999 Time delay in the Kuramoto model of coupled oscillators *Phys Rev Lett* **82** 648-51

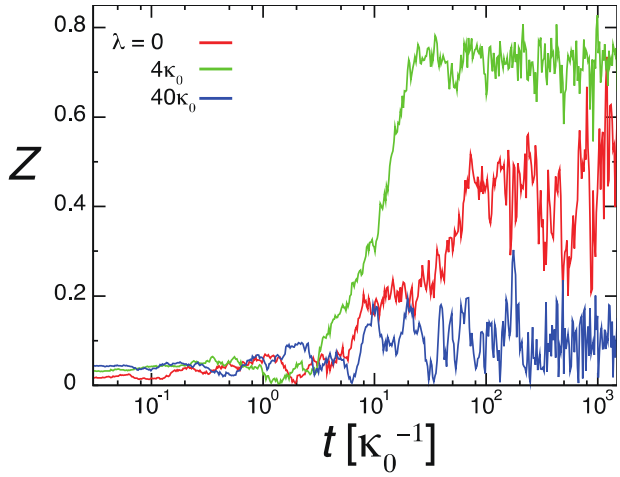

Figure S1. Time evolution of single trajectories of the order parameter for different moving rates λ. Parameters are $\beta = 33\kappa_0$ and $C = 0.25\kappa_0$.

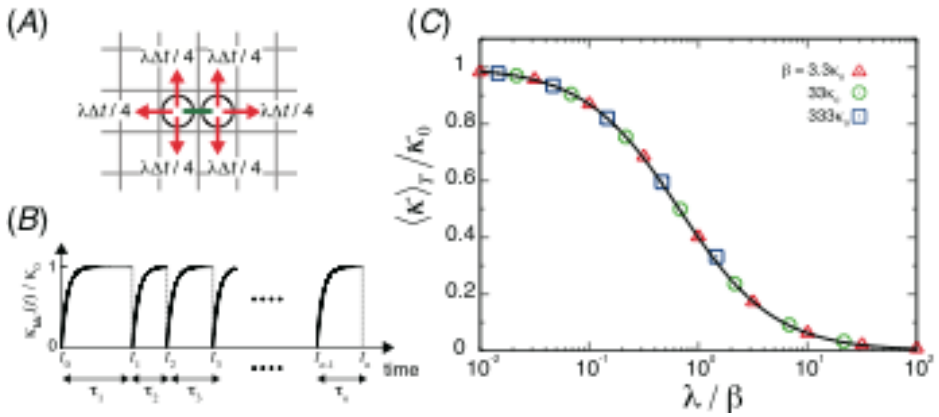

Figure S2. Eq. (5) in the main text agrees with the time average of the coupling strength between two adjacent sites calculated by numerical simulations. (A) The probability that one of two cells in sites **k** and **k'** moves away from the other within small time interval Δt. (B) The time series of the coupling strength between sites **k** and **k'**. (C) Comparison between the time average of the coupling strength between two adjacent sites calculated by numerical simulations with different coupling recovery rate β (symbols), and the effective coupling strength given by Eq. (5) in the main text (solid line).

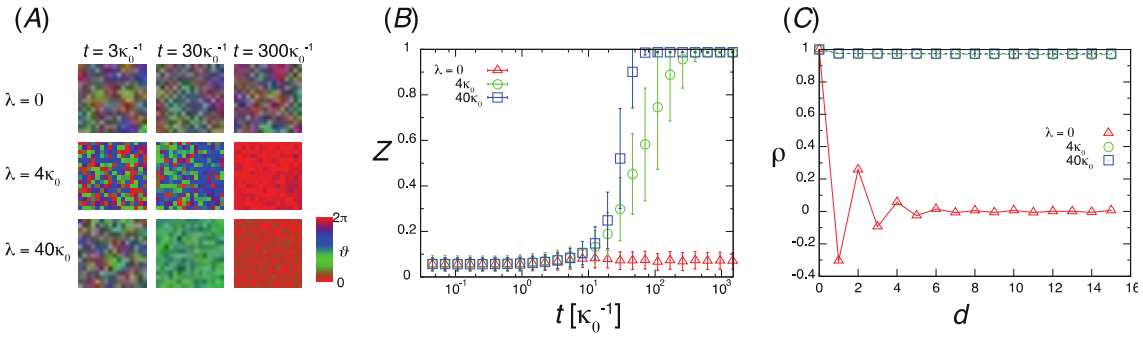

Figure S3. Effects of coupling delay for instantaneous coupling recovery. The degree of synchronization monotonically increases with the increase of the moving rate λ in a model including coupling time delay, Eq. (S.2.1), when coupling recovery is instantaneous, $\beta = \infty$ in Eq. (1b). (A) Snapshots of spatial phase profiles in the two-dimensional lattice at different moving rates λ, observed in numerical simulations of Eq. (S.2.1). The phase ϑ in each site is represented by a color look-up table as indicated. (B) Time evolution of the order parameter $Z(t)$ defined by Eq. (2) in the main text for different moving rates λ. Error bars indicate standard deviations. (C) Dependence of the correlation defined by Eq. (3) in the main text on the distance d between two sites. We plotted the temporal average of the correlation after its value reached a steady state. Error bars for temporal standard deviations are smaller than the size of symbols in (C). $C_d = 0.01\kappa_0$ and other parameters in Eq. (S.2.1) are as described in the supporting information.

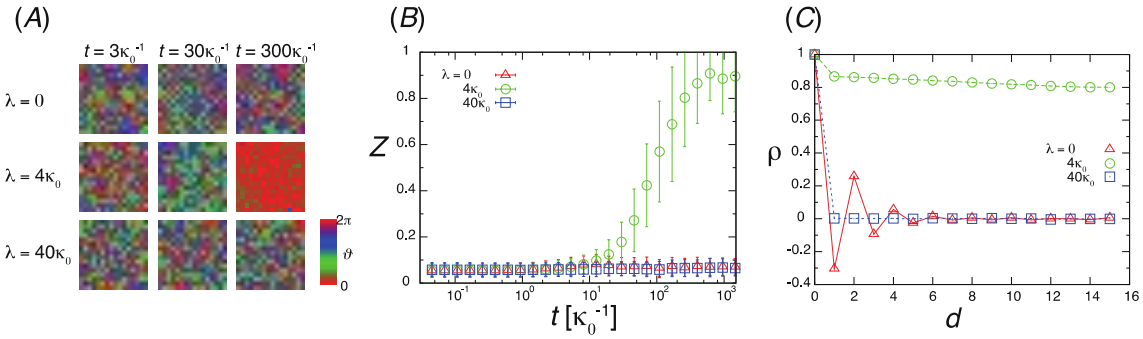

Figure S4. Effects of coupling delay for gradual coupling recovery. Dependence of the degree of synchronization on the moving rate λ is non-monotonic for gradual coupling recovery ($\beta = 33\kappa_0$), in a model including coupling time delay, Eq. (S.2.1). (A) Snapshots of spatial phase profiles in the two-dimensional lattice at different moving rates λ observed in numerical simulations of Eq. (S.2.1). The phase ϑ in each site is represented by a color look-up table as indicated. (B) Time evolution of the order parameter $Z(t)$ defined by Eq. (2) in the main text for different moving rates λ. Error bars indicate standard deviations. (C) Dependence of the correlation defined by Eq. (3) in the main text on the distance *d* between two sites. We plotted the temporal average of the correlation after its value reached a steady state. Error bars for temporal standard deviations are smaller than the size of symbols in (C). In all panels $C_d = 0.01\kappa_0$ and other parameters in Eq. (S.2.1) are as described in the supporting information.

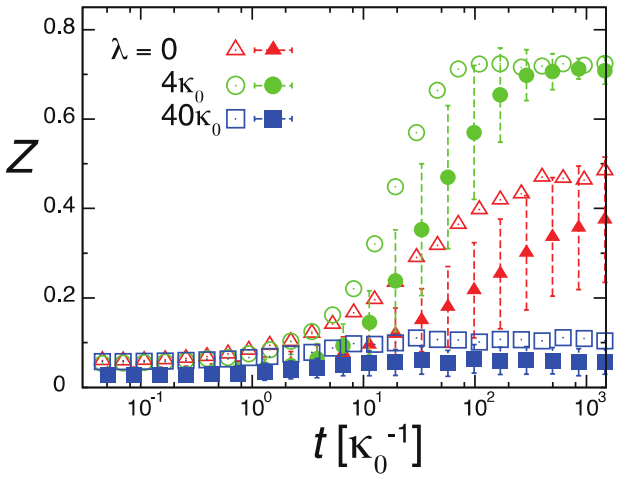

Figure S5. Effects of system size. Time evolution of the order parameter $Z(t)$ defined by Eq. (2) in the main text for different moving rates λ with the system size of 32×32 (filled symbols) and 16×16 (open symbols; data shown in figure 2(*B*) of the main text, plotted for comparison). Error bars of filled symbols indicate standard deviations. Error bars of open symbols are shown in figure 2(*B*) of the main text. Parameters are $\beta=33\kappa_0$ and $C=0.25\kappa_0$.

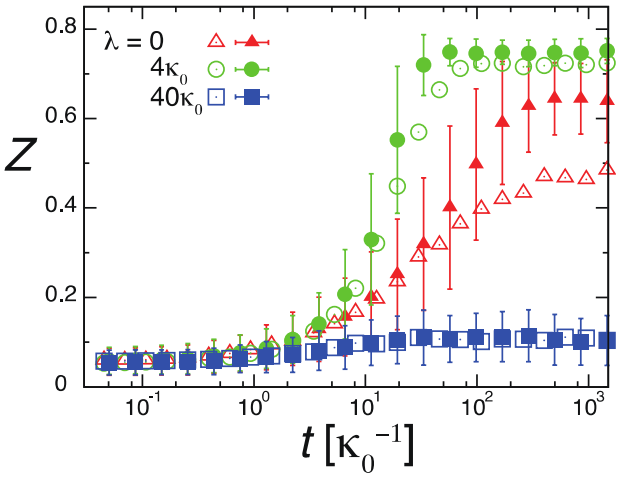

Figure S6. Effects of boundary conditions. Time evolution of the order parameter $Z(t)$ defined by Eq. (2) in the main text for different moving rates λ, with periodic boundary conditions (filled symbols) and open boundary conditions (open symbols; data shown in figure 2(*B*) in the main text, plotted for comparison). Error bars of filled symbols indicate standard deviations. Error bars of open symbols are shown in figure 2(*B*) of the main text. The behavior is qualitatively the same in both cases, showing that the choice of boundary condition does not affect our conclusions. For periodic boundary conditions the system size is effectively smaller, resulting in a quantitative difference for small values of the moving rate λ. Parameters are $\beta = 33\kappa_0$ and $C = 0.25\kappa_0$.

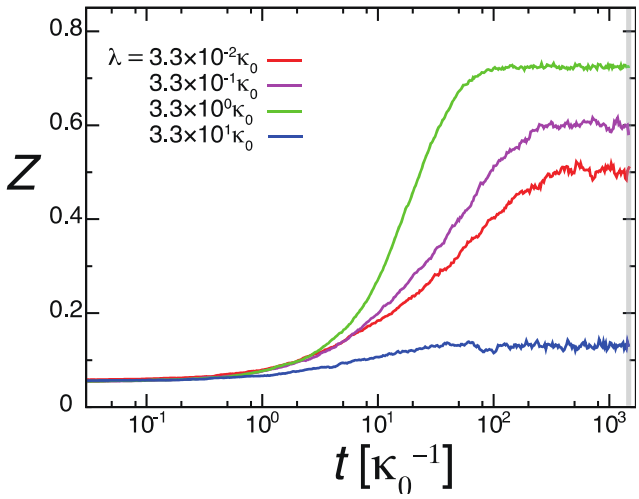

Figure S7. Illustration of steady state measurement of the order parameter as defined by Eq. (2) in the main text. The figure shows the time evolutions of the order parameter in simulations of Eq. (1a) with coupling recovery Eq. (1b) in the main text. The thin gray vertical band spanning from $t=1410\kappa_0^{-1}$ to $t=1500\kappa_0^{-1}$ indicates the time window over which we calculate the time average for this particular steady state measurement. Parameters are $\beta=33\kappa_0$ and $C=0.25\kappa_0$.